

Global quieting of high-frequency seismic noise due to COVID-19 pandemic lockdown measures

Thomas Lecocq 1*, Stephen Hicks 2, Koen Van Noten 1, Kasper van Wijk 3, Paula Koelemeijer 4, Raphael S.M. De Plaen 5, Frédéric Massin 6, Gregor Hillers 7, Robert E. Anthony 8, Maria-Theresia Apoloner 9, Mario Arroyo-Solórzano 10, Jelle D. Assink 11, Pinar Büyükakpınar 12,13, Andrea Cannata 14,15, Flavio Cannavo 15, Sebastian Carrasco 16, Corentin Caudron 17, Esteban J. Chaves 18, David G. Cornwell 19, David Craig 20, Olivier F. C. den Ouden 11,21, Jordi Diaz 22, Stefanie Donner 23, Christos P. Evangelidis 24, Láslo Evers 11,21, Benoit Fauville 25, Gonzalo A. Fernandez 26, Dimitrios Giannopoulos 27,28, Steven J. Gibbons 29, Társilo Girona 30, Bogdan Grecu 31, Marc Grunberg 32, György Hetényi 33, Anna Horleston 34, Adolfo Inza 35, Jessica C.E. Irving 34,36, Mohammadreza Jamalreyhani 37,13, Alan Kafka 38, Mathijs R. Koymans 11,21, Celeste R. Labeledz 39, Eric Larose 17, Nathaniel J. Lindsey 40, Mika McKinnon 41,42, Tobias Megies 43, Meghan S. Miller 44, William Minarik 45,46, Louis Moresi 44, Víctor H. Márquez-Ramírez 5, Martin Möllhoff 20, Ian M. Nesbitt 47,48, Shankho Niyogi 49, Javier Ojeda 50, Adrien Oth 51, Simon Proud 52, Jay Pulli 53,38, Lise Retailleau 54,55, Annukka E. Rintamäki 7, Claudio Satriano 54, Martha K. Savage 56, Shahar Shani-Kadmiel 21, Reinoud Sleeman 11, Efthimios Sokos 57, Klaus Stammler 23, Alexander E. Stott 58, Shiba Subedi 33, Mathilde B. Sørensen 59, Taka'aki Taira 60, Mar Tapia 61, Fatih Turhan 12, Ben van der Pluijm 62, Mark Vanstone 63, Jerome Vergne 64, Tommi A.T. Vuorinen 7, Tristram Warren 65, Joachim Wassermann 43, Han Xiao 66

*Correspondence: thomas.lecocq@seismology.be

1 Seismology-Gravimetry, Royal Observatory of Belgium, Avenue circulaire 3, 1180 Brussels, Belgium

2 Department of Earth Science and Engineering, Imperial College London, London, United Kingdom

3 Department of Physics, University of Auckland, New-Zealand

4 Department of Earth Sciences, Royal Holloway University of London, Egham, United Kingdom

5 Centro de Geociencias, Universidad Nacional Autónoma de México, Campus Juriquilla, Querétaro, Mexico

6 Swiss Seismological Service, ETH Zurich, Sonneggstrasse 5, CH-8092, Zurich, Switzerland

7 Institute of Seismology, University of Helsinki, Helsinki, Finland

8 U.S. Geological Survey - Albuquerque Seismological Laboratory, New Mexico, United States of America

9 Zentralanstalt für Meteorologie und Geodynamik (ZAMG), Vienna, Austria

10 Escuela Centroamericana de Geología, Universidad de Costa Rica, San José, Costa Rica

11 R&D Seismology and Acoustics, Royal Netherlands Meteorological Institute (KNMI), Utrechtseweg 297, 3731 GA De Bilt, The Netherlands

12 Kandilli Observatory and Earthquake Research Institute, Boğaziçi University, Istanbul, Turkey

13 GFZ German Research Centre for Geosciences, Potsdam, Germany

14 Dipartimento di Scienze Biologiche, Geologiche e Ambientali, Università Degli Studi di Catania, Catania, Italy

15 Istituto Nazionale di Geofisica e Vulcanologia, Osservatorio Etneo, Catania, Italy

16 Bensberg Observatory, University of Cologne, Cologne, Germany

17 Univ. Grenoble Alpes, Univ. Savoie Mont Blanc, CNRS, IRD, IFSTTAR, ISTERRE, 38000 Grenoble, France

18 Volcanological and Seismological Observatory of Costa Rica at Universidad Nacional (OVSICORI-UNA), Costa Rica

19 Department of Geology & Geophysics, School of Geosciences, University of Aberdeen, King's College, Aberdeen, AB24 3UE, United Kingdom

20 Dublin Institute for Advanced Studies, Geophysics Section, 5 Merrion Square, D02 Y006 Dublin, Ireland

21 Dept. of Geoscience and Engineering, Delft University of Technology, Stevinweg 1, 2628 CN Delft, The Netherlands

22 Geosciences Barcelona, CSIC, Barcelona, Spain

23 Federal Institute for Geosciences and Natural Resources (BGR), Hannover, Germany

24 Institute of Geodynamics, National Observatory of Athens

25 Noise Department, Brussels Environment, Brussels-Capital Region, Belgium

26 Observatorio San Calixto, Bolivia

27 Seismotech S.A., Athens, Greece
28 Hellenic Mediterranean University, Dept. of Environmental & Natural Resources Engineering, Laboratory of Geophysics & Seismology, Chania, Greece
29 Norges Geotekniske Institutt, Sognsveien 72, 0855 Oslo, Norway
30 Geophysical Institute, University of Alaska Fairbanks, Alaska 99775, United States of America
31 National Institute for Earth Physics, Calugareni 12, Magurele, Romania
32 Réseau National de Surveillance Sismique (RENASS); Université de Strasbourg, CNRS, EOST UMS830, 5 rue René Descartes, F-67084 Strasbourg Cedex, France
33 Institute of Earth Sciences, Faculty of Geosciences and Environment, University of Lausanne, Lausanne, Switzerland
34 School of Earth Sciences, University of Bristol, Queen's Road, Bristol, BS8 1RJ, United Kingdom
35 Instituto Geofísico del Perú, Lima, Peru
36 Department of Geosciences, Princeton University, NJ, United States of America
37 Institute of Geophysics, University of Tehran, Iran
38 Weston Observatory, Department of Earth and Environmental Sciences, Boston College, Weston, MA, United States of America
39 Seismological Laboratory, California Institute of Technology, Pasadena, CA, United States of America
40 Geophysics Department, Stanford University, Stanford, CA, United States of America
41 SETI Institute, Mountain View, CA, USA
42 Faculty of Science, Department of Earth, Ocean and Atmospheric Sciences, University of British Columbia
43 Ludwig-Maximilians-Universität München, Munich, Germany
44 Research School of Earth Sciences, Australian National University, Canberra, ACT Australia
45 Department of Earth and Planetary Sciences, McGill University & GEOTOP Research Centre, Montréal, QC, Canada
46 GEOTOP Research Centre, Montréal, QC, Canada
47 Raspberry Shake, S.A.
48 Department of Earth and Climate Science, University of Maine, Orono, ME, United States of America
49 University of California, Riverside, United States of America
50 Departamento de Geofísica, Universidad de Chile, Santiago, Chile
51 European Center for Geodynamics and Seismology; 19, rue Josy Welter; L-7256 Walferdange, Grand Duchy of Luxembourg
52 National Centre for Earth Observation, Department of Physics, University of Oxford
53 Raytheon BBN Technologies, Arlington, VA, United States of America
54 Université de Paris, Institut de physique du globe de Paris, CNRS, F-75005 Paris, France
55 Observatoire Volcanologique du Piton de la Fournaise, Institut de physique du globe de Paris, F-97418 La Plaine des Cafres, France
56 School of Geography, Environment and Earth Sciences, Victoria University of Wellington, New Zealand
57 Department of Geology, University of Patras, Patras, 26504 Rio, Greece
58 Department of Electrical and Electronic Engineering, Imperial College London, South Kensington Campus, London, SW7 2AZ, United Kingdom
59 Department of Earth Science, University of Bergen, Bergen, Norway
60 Berkeley Seismological Laboratory, University of California Berkeley, Berkeley, United States of America
61 Laboratori d'Estudis Geofísics Eduard Fontserè, Institut d'Estudis Catalans (LEGEF-IEC), Barcelona, Spain
62 Department of Earth and Environmental Sciences, University of Michigan-Ann Arbor, MI, United States of America
63 Geology Department, Truro School, Trennick Lane, Truro, Cornwall, TR1 1TH, United Kingdom
64 Institut de Physique du Globe de Strasbourg ; UMR 7516, Université de Strasbourg/EOST, CNRS ; 5 rue René Descartes, F-67084 Strasbourg Cedex, France
65 Department of Physics, University of Oxford, United Kingdom
66 Department of Earth Science and Earth Research Institute, University of California, Santa Barbara, CA, United States of America

ABSTRACT: Human activity causes vibrations that propagate into the ground as high-frequency seismic waves. Measures to mitigate the COVID-19 pandemic caused widespread changes in human activity, leading to a months-long reduction in seismic noise of up to 50%. The 2020 seismic noise quiet period is the longest and most prominent global anthropogenic seismic noise reduction on record. While the reduction is strongest at surface seismometers in populated areas, this seismic quiescence extends for many kilometers radially and hundreds of meters in depth. This provides an opportunity to detect subtle signals from subsurface seismic sources that would have been concealed in noisier times and to benchmark sources of anthropogenic noise. A strong correlation between seismic noise and independent measurements of human mobility suggests that seismology provides an absolute, real-time estimate of population dynamics.

ONE SENTENCE SUMMARY: Global changes in social and economic activity following COVID-19 lockdown measures caused significantly lower anthropogenic seismic noise levels.

Seismometers record signals from more than just earthquakes; interactions between the solid Earth and fluid bodies, such as ocean swell and atmospheric pressure (1,2), are now commonly used to image and monitor the subsurface (3). Human activity is a third source of seismic signal. Nuclear explosions and fluid injection/extraction result in impulsive signals, but everyday human activity is recorded as near-continuous signal especially on seismometers in urban environments. These complicated signals are the superposition of a wide variety of activities happening at different times and places at or near the Earth's surface, but are typically stronger during the day than at night, weaker on weekends than weekdays, and stronger near population centers (4,5,6,7). Seismometers in urban environments are important to maximize the spatial coverage of seismic networks and to warn of local geologic hazards (8), even though anthropogenic seismic noise degrades their capability to detect transient signals associated with earthquakes and volcanic eruptions. Understanding urban seismic sources is therefore vital. However, research studies have been limited to confined areas or distinct events, such as road traffic (9,10), public transport (11,7), and "football quakes" (11,12). Broad analysis of the long-term global anthropogenic seismic wavefield has been lacking. The impact of large, coherent changes in human behavior on seismic noise is unknown, as is how far it propagates and whether seismic recordings offer a coarse proxy for monitoring human activity patterns. Answering these questions has proven challenging: datasets are large, monitoring network heterogeneous, and the many possible noise sources likely vary spatially and overlap in time (13).

The COVID-19 outbreak was declared a global health emergency in January 2020 (14) and a pandemic in March by the World Health Organisation. The outbreak resulted in emergency measures to reduce the basic reproduction rate of the virus (R_0) (15), beginning in China, Italy, and then followed by most countries. These measures disrupted social and economic behavior (16), industry (17), and tourism (18). In this paper, we use "lockdown" to broadly encompass many types of emergency measures, such as full quarantine (e.g. Wuhan, China (19,20,21)), enforced physical distancing (e.g. Italy; UK), travel restrictions (22), widespread closure of services and industry, or any other emergency measures. These drastic changes to daily life provide a unique opportunity to study their environmental impacts, such as reductions in nitrous oxide emissions in the atmosphere (23). Recordings of human-generated seismic vibrations that travel through the solid Earth provide insights into the dynamics of pandemic lockdowns.

We assessed the effects of COVID-19 lockdowns on high-Frequency (4–14 Hz) Seismic Ambient Noise (hiFSAN; (24)). We compiled a global seismic noise dataset using vertical-component seismic waveform data from 337 broadband and individually-operated citizen seismometer stations (24), such as Raspberry Shakes (RS), with a self-noise well below the ground motion generated by anthropogenic noise (25), and flat responses in the target frequency band (Fig. 1). For 268 seismic stations, we obtained usable data (e.g. no large data gaps, working sensors) and found significant reductions in hiFSAN during local lockdown measures at 185 stations (Fig. 2). Periods that are often seismically quiet include weekends, and the Christmas / New Year holidays for those locations where these are celebrated. We found a near-global reduction in noise, commencing in China in late Jan 2020, then followed by Europe and the rest of the world in Mar to Apr 2020. The noise level we observe during lockdowns lasted longer and was often quieter than the Christmas to New Year period.

In China (Fig. 3A), the COVID-19 outbreak and subsequent emergency measures occurred

during Chinese New Year (CNY). In Enshi city, Hubei province, where the outbreak began (26), hiFSAN in 2020 clearly diverges from the normal annual reduction during CNY. The hiFSAN level remained at a minimum for several weeks after CNY. This minimum was demarcated by the start and end of quarantine in Hubei. While such strict quarantine measures were not enforced in Beijing, local hiFSAN reductions are stronger and longer than recent years. As of the end date of our analysis, Beijing has still not reached the average hiFSAN level of previous years, suggesting the impact of COVID-19 is still restricting anthropogenic noise there. We noticed a later hiFSAN lockdown reduction in Apr 2020 in Heilongjiang, in NE China, near the Russian border.

While we see seismic effects of lockdown in areas with low population density estimates (<1 person per km^2 , Fig. 1), the strongest hiFSAN reduction occurs in populated environments. For a permanent seismic station in Sri Lanka, a 50% reduction in hiFSAN occurred after lockdown, the strongest we observed in the available data from that station since at least July 2013 (Fig. S2). In Central Park, New York, on Sunday nights, hiFSAN was 10% lower during the lockdown compared to before it (Fig. S3).

Seismic networks in populated areas allow us to correlate hiFSAN with other human activity measurements, such as audible recordings and flight data (24). At a surface station in Brussels, Belgium (Fig. 3B), we found a 33% reduction in hiFSAN after lockdown. We compared this with data from a nearby microphone, located close to a major road, that mainly records audible traffic noise. We found a high correlation between pre-lockdown hiFSAN and audible noise, both showing characteristic diurnal and weekly changes. However, during lockdown, audible noise reductions are more pronounced, suggesting that seismometers are sensitive to a wider distribution of seismic sources, not solely to the nearby traffic. Audible and hiFSAN levels then gradually increase after Apr 2020. Independent mobility data (24) provide insights into what cause these changes. Mobility correlates with hiFSAN at lockdown, with correlation coefficients exceeding 0.8 (24), except for time spent at places of residence (Google's "residential" category), which is expected given the increased number of people spending more time at home due to government restrictions.

Citizen seismometers provide a different urban ground motion dataset, with denser coverage in some places. Large hiFSAN drops especially occurred at schools and universities following lockdown-related closures (e.g. in Boston and Michigan (US) and Cornwall (UK)), Fig. S4). The hiFSAN level is even 20% lower than during school holidays, indicating sensitivity to the environment outside of the school.

The pandemic impacted tourism, for example, during the holiday season in the Caribbean. In Barbados (Fig. 3C), hiFSAN decreased by $\sim 45\%$ following lockdown on 28 March 2020, through April 2020 and stayed $\sim 50\%$ below levels observed in previous years for the same period. However, seismic noise levels started to decrease 1–2 weeks before a local curfew started. Local flight data (24) imply travel to Barbados started decreasing after 21 March 2020 and the overall reduction in hiFSAN might be due in part to tourists repatriating. We also observed noise reductions due to reduced tourist activity at ski resorts in Europe (Zugspitze) and the US (Mammoth Mountain) (Fig. S5).

While we saw lockdown effects most strongly at surface stations, we also detected them underground. Seismometers installed in boreholes to minimize the effects of anthropogenic noise on the data monitor potential hazards associated with the Auckland Volcanic Field, New Zealand (27,8,6). Station HBAZ is 380 m below the city, while MBAZ is at 98 m depth, 14 km from

the city center on the uninhabited Motutapu island (Fig. 3D). The hiFSAN level at both stations varies between weekdays and weekends before the lockdown, suggesting that both are sensitive to anthropogenic activity. While the island station is quieter overall, the lockdown instigated a reduction in hiFSAN by a factor of two for both stations. We attribute the remaining hiFSAN maxima on the island (mid Apr 2020; early May 2020) to strong winds and high waves. On 27 April 2020, New Zealand lifted restrictions, with hiFSAN increasing to the pre-lockdown levels.

The reduction of hiFSAN is weaker in less populated areas, such as at Rundu which is located along the Namibia-Angola border (Fig. 3E). After COVID-19 was confirmed in Namibia, an emergency was declared on 17 Mar 2020 to restrict mobility, followed by full lockdown on 27 Mar 2020. These measures are reflected in $>25\%$ hiFSAN reduction compared to pre-lockdown. Despite Rundu having a population roughly eight and five times less dense than Brussels and Auckland, respectively (28), we observed a similarly high correlation between seismic and mobility data. The Black Forest Observatory in Germany is an even more remote station, located 150–170 m below the surface in crystalline bedrock. Considered a reference low-noise laboratory (29), even there we found a small hiFSAN reduction during lockdown nights (Fig. S6), corresponding to the lowest hiFSAN since at least 25 Dec 2015.

We have provided a global-scale analysis of high-frequency anthropogenic seismic noise. Global median hiFSAN dropped by as much as 50% during March to May 2020 (Fig. 4). The length and quiescence of this period represents the longest and most coherent global seismic noise reduction in recorded history, highlighting how human activities impact the solid Earth. A globally high correlation exists between changes in hiFSAN and population mobility (24), with correlations exceeding 0.9 for many categories.

This distinct low-noise period will help to optimize seismic monitoring (4). Analyzing the full spectrum of seismogenic behavior, including the smallest earthquakes, is essential for monitoring fault dynamics over seismic cycles, and for earthquake forecasting and seismic hazard assessment. Small earthquakes should dominate datasets (30), but typical operational catalogues using amplitude-based detection lack many of the smallest earthquakes (31). This detection issue is especially problematic in populated areas, where anthropogenic noise energy interferes with earthquake signals. This problem is exemplified by recordings of a M5.0 earthquake at 15 km depth SW of Petatlan, Mexico during lockdown (Fig. S7). An earthquake with this magnitude and source mechanism occurring during daytime could typically only be observed at stations in urban environments by filtering the signal. However, the reduction of seismic noise by $\sim 40\%$ during lockdown made this event visible without any filtering required at a RS station in Querétaro city, 380 km away. Low noise levels during COVID-19 lockdowns could thus allow detection of signals from new sources in areas with incomplete seismic catalogues. Such newly identified signals could be used as distinct templates (30) for finding similar waveforms in noisier data pre- and post-lockdown. This approach also works for tremor signals masked by anthropogenic noise, yet vital for monitoring potential volcanic unrest (6). Although broadband sensors in rural environments are impacted less by anthropogenic noise, any densification of and reliance on low-cost sensors in urban areas, such as RS and low-cost accelerometers (32), will require a better understanding of anthropogenic noise sources to suppress false detections. As populations increase globally, more people become exposed to potential natural and induced geohazards (33). Urbanization will increase anthropogenic noise in exposed areas, further complicating seismic monitoring. Characterizing and minimizing anthropogenic noise is increasingly important

for accurately detecting and imaging the seismic signatures of potentially harmful subsurface hazards.

Anthropogenic seismic noise is thought to be dominated by noise sources less than 1 km away (34,5,6,7,11). Because population mobility generates time-varying loads that radiate energy through the shallow subsurface as Rayleigh waves (11), local effects, such as construction sites, heavy machinery, can impact individual stations. However, the unique 2020 seismic noise quiet period reveals that when considering multiple stations or whole networks over longer time-scales, the anthropogenic seismic wavefield affects large areas. With denser networks and more citizen sensors in urban environments, more features of the seismic noise, rather than just amplitude, will become usable and will help to identify different anthropogenic noise sources (35,10). Characterizing these sources will be useful for imaging the shallow subsurface in 3D in urban areas using high-frequency anthropogenic ambient noise (36,37). Our finding of a distributed noise field is supported by the strong correlations with independent mobility data (Fig. 4). In contrast to mobility data, publicly available data from existing seismometer networks provide an objective absolute baseline of human activity levels. Therefore, hiFSAN can serve as a near-real-time technique for monitoring anthropogenic activity patterns with fewer potential privacy concerns than mobility data. In addition, industrial activities may not be captured in mobility data, but leave a seismic noise signature. The 2020 seismic quiet period is a baseline for using seismic properties (34) to identify and isolate the sources contributing to the anthropogenic noise wavefield, especially when combined with data indicative of human behavior. The seismic observations of human activity during the COVID-19 lockdown allow us to assess the impact of mitigation policies on daily life, especially the time to establish and recover from lockdowns. As such, hiFSAN may provide important constraints for health and behavioral science studies.

References

- (1) J. N. Brune, J. Oliver, *Bulletin of the Seismological Society of America* **49**, 349 (1959).
- (2) R. K. Cessaro, *Bulletin of the Seismological Society of America* **84**, 142 (1994).
- (3) N. M. Shapiro, M. Campillo, *Geophysical Research Letters* **31**, 7 (2004).
- (4) D. E. McNamara, R. P. Buland, *Bulletin of the Seismological Society of America* **94**, 1517 (2004).
- (5) J. C. Groos, J. R. Ritter, *Geophysical Journal International* **179**, 1213 (2009).
- (6) C. M. Boese, L. Wotherspoon, M. Alvarez, P. Malin, *Bulletin of the Seismological Society of America* **105**, 285 (2015).
- (7) D. N. Green, I. D. Bastow, B. Dashwood, S. E. Nippress, *Seismological Research Letters* **88**, 113 (2017).
- (8) C. L. Ashenden, et al., *Natural Hazards* **59**, 507 (2011).
- (9) N. Riahi, P. Gerstoft, *Geophysical Research Letters* **42**, 2674 (2015).
- (10) N. J. Lindsey, et al., arXiv preprint arXiv:2005.04861 (2020).
- (11) J. Díaz, M. Ruiz, P. S. Sánchez-Pastor, P. Romero, *Scientific Reports* **7**, 1 (2017).
- (12) P. Denton, S. Fishwick, V. Lane, D. Daly, *Seismological Research Letters* **89**, 1902 (2018).
- (13) D. Wilson, et al., *Bulletin of the Seismological Society of America* **92**, 3335 (2002).
- (14) C. Sohrabi, et al., *International Journal of Surgery* (2020).
- (15) R. M. Anderson, H. Heesterbeek, D. Klinkenberg, T. D. Hollingsworth, *The Lancet* **395**, 931 (2020).
- (16) M. Nicola, et al., *International Journal of Surgery* (2020).
- (17) T. Laing, *The Extractive Industries and Society* (2020).
- (18) A. Hoque, F. A. Shikha, M. W. Hasanat, I. Arif, A. B. A. Hamid, *Asian Journal of Multidisciplinary Studies* **3**, 52 (2020).
- (19) M. U. G. Kraemer, et al., *Science* **368**, 493 (2020).
- (20) H. Tian, et al., *Science* **368**, 638 (2020).
- (21) J. Zhang, et al., *Science* **368**, 1481 (2020).
- (22) M. Chinazzi, et al., *Science* **368**, 395 (2020).
- (23) M. Bauwens, et al., *Geophysical Research Letters* **47**, 11 (2020).
- (24) Materials and Methods, and Network Citations are available as supplementary materials on Science Online.
- (25) R. E. Anthony, A. T. Ringler, D. C. Wilson, E. Wolin, *Seismological Research Letters* **90**, 219 (2019)
- (26) H. Lau, et al., *Journal of Travel Medicine* (2020).
- (27) S. Sherburn, B. J. Scott, J. Olsen, C. Miller, *New Zealand Journal of Geology and Geophysics* **50**, 1 (2007).
- (28) Center for International Earth Science Information Network CIESIN Columbia University, Gridded population of the world, version 4 (GPWv4): Population density, Revision 11 (2018). <https://doi.org/10.7927/H49C6VHW>. Accessed 2 June 2020.
- (29) W. Zürn, et al., *Geophysical Journal International* **171**, 780 (2007).
- (30) B. Gutenberg, C. F. Richter, *Bulletin of the Seismological Society of America* **34**, 185 (1944).
- (31) Z. E. Ross, D. T. Trugman, E. Hauksson, P. M. Shearer, *Science* **364**, 767 (2019).

- (32) E. S. Cochran, *Nature Communications* **9**, 1 (2018).
- (33) G. McCall, Geological Society, London, *Engineering Geology Special Publications* **15**, 309 (1998).
- (34) M. Lehujeur, J. Vergne, J. Schmittbuhl, A. Maggi, *Geothermal Energy* **3**, 3 (2015).
- (35) G. Hillers, M. Campillo, Y.-Y. Lin, K.-F. Ma, P. Roux, *Journal of Geophysical Research: Solid Earth* **117** (2012).
- (36) M. Picozzi, S. Parolai, D. Bindi, A. Strollo, *Geophysical Journal International* **176**, 164 (2009).
- (37) F. Brenguier, et al., *Geophysical Research Letters* **46**, 9529 (2019).

Acknowledgments

We sincerely thank the editor Brent Grocholski, two anonymous reviewers and Tarje Nissen-Meyer for their comments, which have improved the manuscript. We are extremely grateful to all seismic network managers, operators, and technicians who have helped to facilitate the raw global seismic dataset (24). We also kindly acknowledge all the passionate community seismologists for running their "home" seismometers and participating, indirectly, to a better understanding of the Earth. Any use of trade, firm, or product names is for descriptive purposes only and does not imply endorsement by the U.S. Government. We dedicate this community-led study to all essential workers who have kept our countries going during these difficult times.

Funding:

- P.K. was funded by a Royal Society University Research Fellowship (URF\R1\180377).
- P.B. and M.J. acknowledge support from the International Training Course "Seismology and Seismic Hazard Assessment" funded by the GeoForschungsZentrum Potsdam (GFZ) and the German Federal Foreign Office through the German Humanitarian Assistance program (grant S08-60 321.50 ALL 03/19).
- P.B. also acknowledges financial support from the Boğaziçi University Research Fund (BAP 15683).
- O.F.C.d.O acknowledges funding from a Young Investigator Grant from the Human Frontier Science Program (HFSP - project number RGY0072/2017).
- C.P.E. and E.S. acknowledge funding from the HELPOS Project "Hellenic Plate Observing System" (MIS 5002697).
- L.E. and S.S.-K. acknowledge funding from a VIDI project from the Dutch Research Council (NWO project number 864.14.005).
- G.A.F. acknowledges contributions from the Observatorio San Calixto, which is supported by the Air Force Technical Application Center (AFTAC).
- C.R.L. acknowledge funding from the NSF Graduate Research Fellowship Program (grant No. DGE-1745301).
- V.-H.M. and R.D.P. acknowledge support from grant CONACYT-299766.
- R.D.P. acknowledges support from the UNAM-DGAPA postdoctoral scholarship.
- J.O. acknowledges support from the Agencia Nacional de Investigación y Desarrollo (Scholarship ANID-PFCHA / Doctorado Nacional / 2020-21200903).
- S.P. acknowledges financial support from the Natural Environment Research Council (NE/R013144/1).
- A.E.R. acknowledges support from the K.H. Renlund foundation.
- M.K.S. acknowledges the New Zealand Earthquake Commission (EQC Project No 20796).
- H.X. acknowledges support from a Multidisciplinary Research on the Coronavirus and its Impacts (MRCI) grant from UC Santa Barbara.
- The Australian Seismometers in Schools data used in this research is supported by AuScope, enabled by the Australian Commonwealth NCRIS program.

Authors contributions: TL designed and led the research; TL, SH, KVN, KvW, PK and RDP processed and visualized the data and drafted the manuscript; FM contributed to the software development and provided the Supplementary video; GH thoroughly edited and reviewed the

manuscript. All 76 authors processed seismic data, took part in discussions and performed a full interactive review of the original and revised manuscripts.

Competing interests: The authors declare no competing interests.

Data and materials availability: The raw data used to compute the hiFSAN was obtained from different networks and data providers (24). The computed data and codes used to analyze and plot the Figures 1, 2, 3 and 4 are available from the companion repository:

https://github.com/ThomasLecocq/2020_Science_GlobalQuieting (last accessed July 2020)

Supplementary Materials

Materials and Methods

Supplementary Text (including Network Citations)

Figs. S1 to S9

References (38-55)

Supplementary Files: Tables S1-S3 and Movie M1.

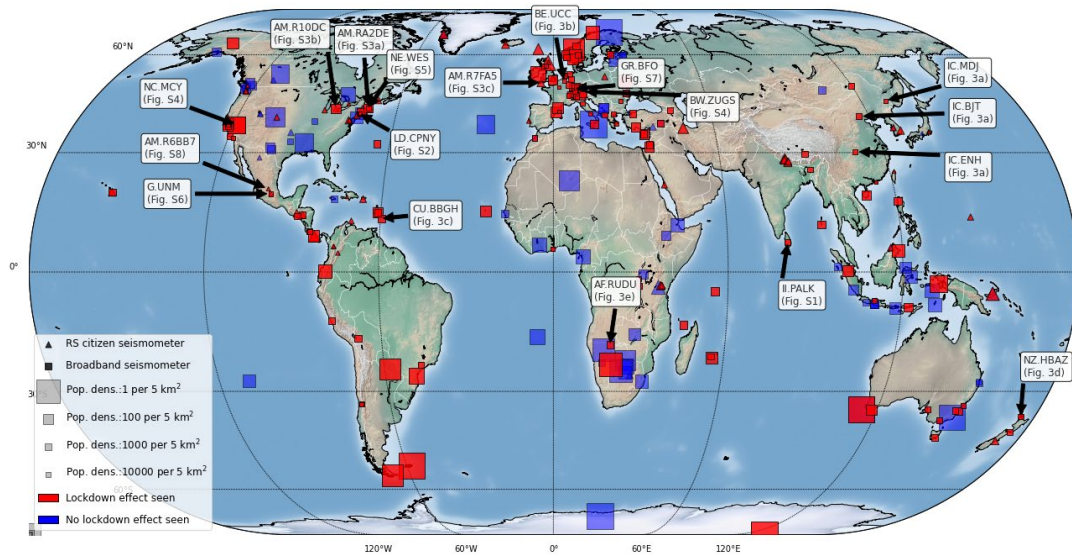


Figure 1: Worldwide seismic station locations.

Locations of the 268 global seismic stations with usable data (e.g. no long data gaps, working sensors) we analyzed. Lockdown effects are observed (red) at 185 out of 268 stations. Symbol size is scaled by the inverse of population density (28) to emphasize stations located in remote areas. The stations we labelled are discussed in detail in the text.

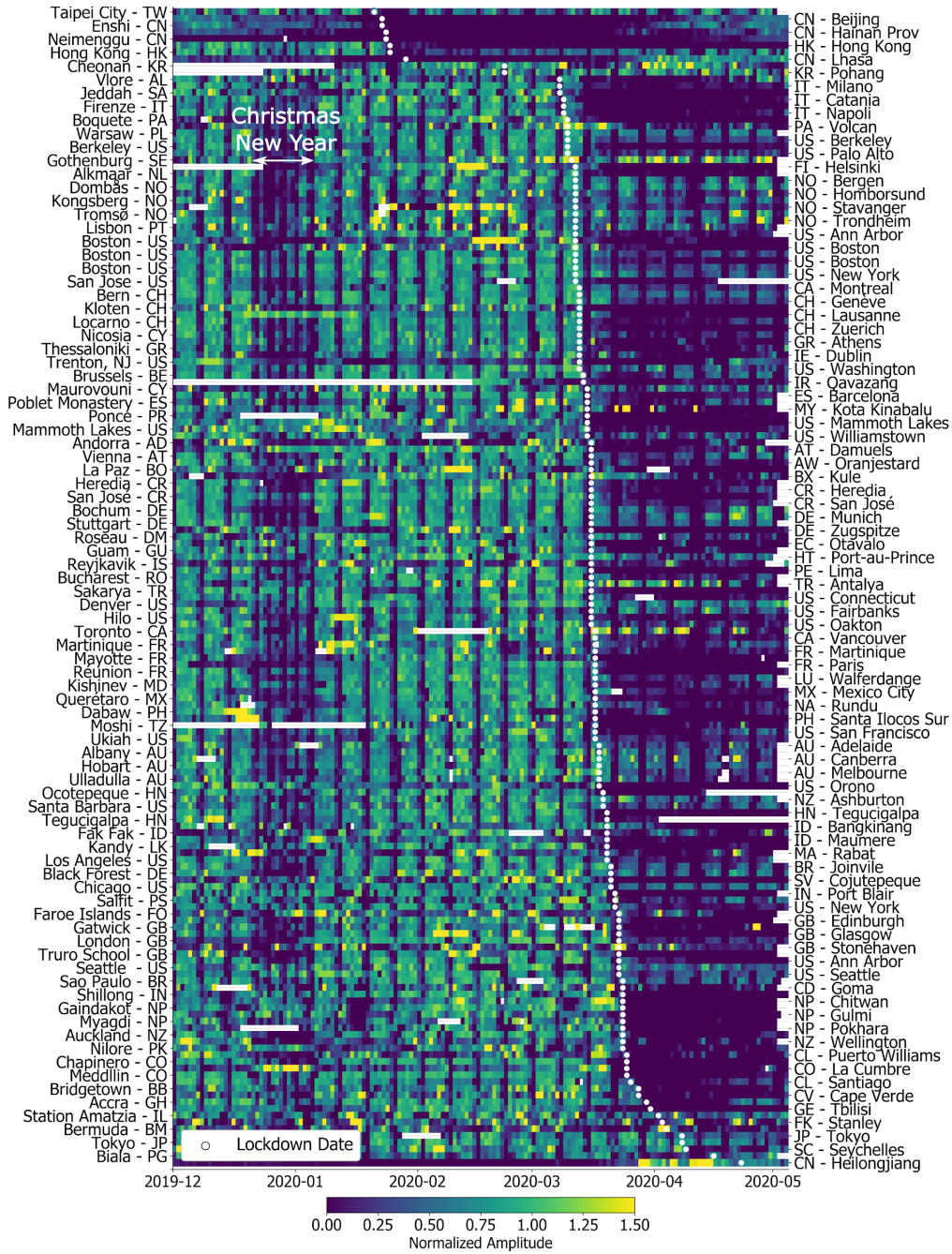


Figure 2: Global temporal changes in seismic noise.

Global daily median hiFSAN based on displacement data (24), normalized to percentage variation of the baseline before lockdown measures, and sorted by lockdown date. Data gaps are colored white. Location and country code of the station are indicated, while Fig. S1 also includes the network and station code.

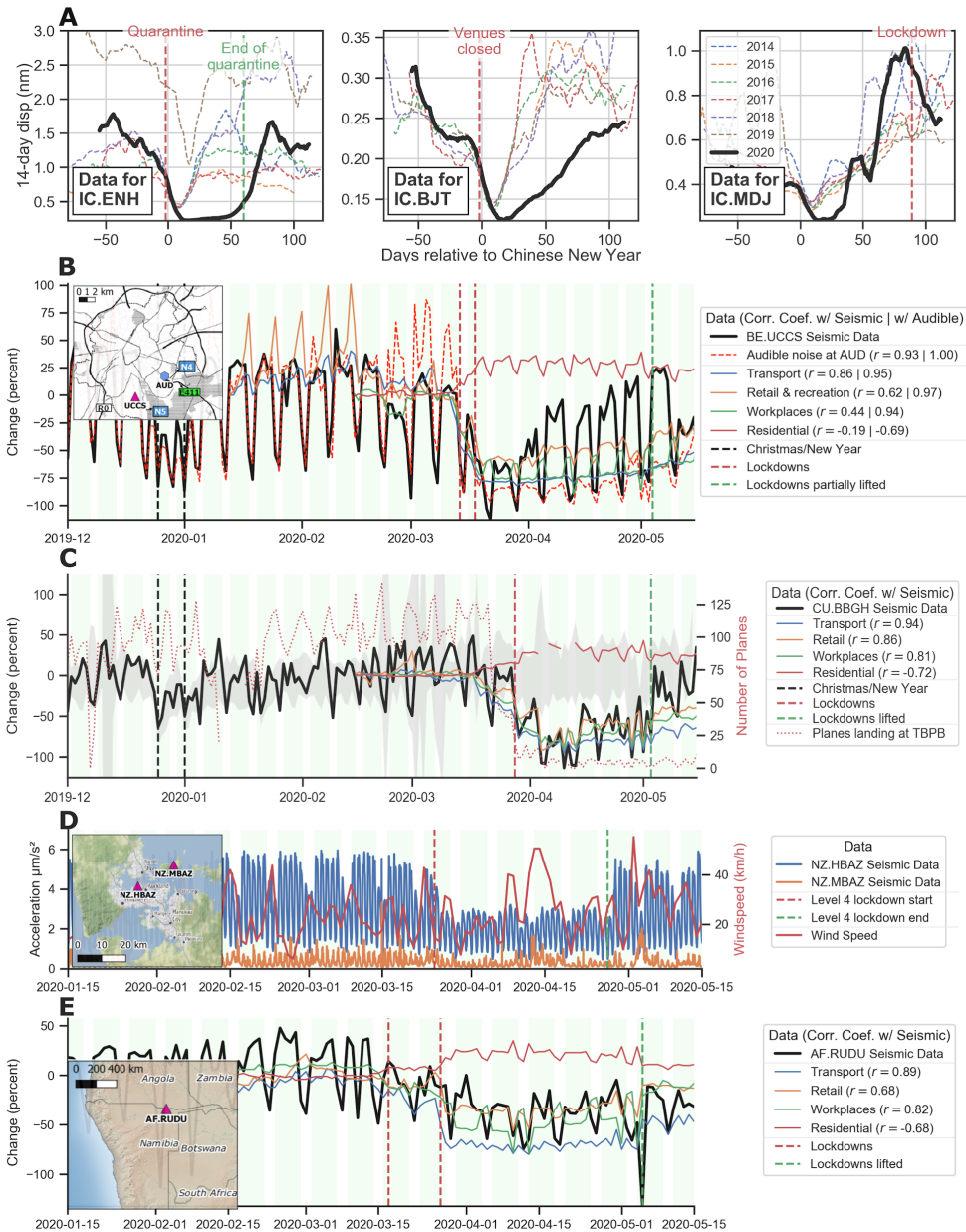


Figure 3: Regional examples of the 2020 seismic noise quiet period.

Examples showing different features of the lockdown seismic signal changes in regional settings. We filtered the hiFSAN data between 4 and 14 Hz and present temporal changes either as displacement (A), acceleration (D) or as percentage change compared to the baseline before lockdown (B, C and E) with the panels in (A) also comparing to the baseline of corresponding time periods in prior years. Individual seismic stations are identified by network.station codes (IC.ENH, BE.UCCS, etc.). The legends of (B-E) include correlation coefficients r with mobility data (24). (A) Lockdown effects at three stations in China compared to the Chinese New Year holiday in previous years. (B) Lockdown effects in hiFSAN compared with audible environmental noise and independent mobility data in Brussels, Belgium. (C) Lockdown effect in Barbados compared to noise levels in the last decade (in grey) and

correlation with local flight data at the Grantley Adams International Airport (TBPB) (24). (D)
Lockdown noise reduction recorded on borehole seismometers in Auckland, New Zealand. (E)
Lockdown noise reduction in a region of low population density in Rundu, Namibia.

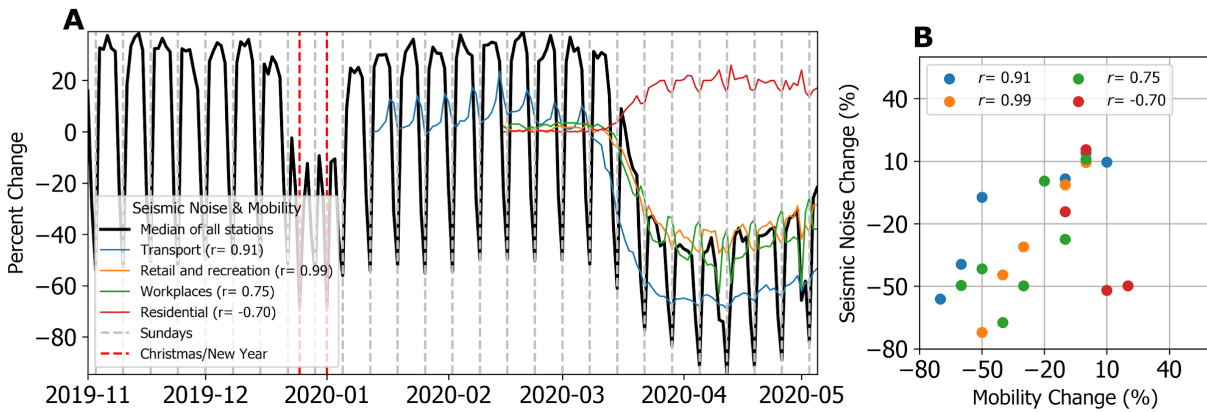


Figure 4: Global changes in seismic noise compared to population mobility trends.

(A) Comparison between temporal changes in global daily median hiFSAN based on the 185 stations that observed lockdown effects and population mobility changes (24). (B) Scatter plot to illustrate the correlation between the binned (10% bins) time series of seismic noise changes and all categories of mobility data in (A). Percentage changes are given relative to a pre-lockdown baseline. All categories show a strong positive correlation, apart from time spent in residential premises, which is anti-correlated.



Supplementary Materials for

Global quieting of high-frequency seismic noise due to COVID-19 pandemic lockdown measures

Thomas Lecocq*, Stephen Hicks, Koen Van Noten, Kasper van Wijk, Paula Koelemeijer, Raphael S.M. De Plaen, Frédéric Massin, Gregor Hillers, Robert E. Anthony, Maria-Theresia Apoloner, Mario Arroyo-Solórzano, Jelle D. Assink, Pinar Büyükakpınar, Andrea Cannata, Flavio Cannavo, Sebastian Carrasco, Corentin Caudron, Esteban J. Chaves, David G. Cornwell, David Craig, Olivier F. C. den Ouden, Jordi Diaz, Stefanie Donner, Christos P. Evangelidis, Láslo Evers, Benoit Fauville, Gonzalo A. Fernandez, Dimitrios Giannopoulos, Steven J. Gibbons, Társilo Girona, Bogdan Grecu, Marc Grunberg, György Hetényi, Anna Horleston, Adolfo Inza, Jessica C.E. Irving, Mohammadreza Jamalreyhani, Alan Kafka, Mathijs R. Koymans, Celeste R. Labeledz, Eric Larose, Nathaniel J. Lindsey, Mika McKinnon, Tobias Megies, Meghan S. Miller, William Minarik, Louis Moresi, Víctor H. Márquez-Ramírez, Martin Möllhoff, Ian M. Nesbitt, Shankho Niyogi, Javier Ojeda, Adrien Oth, Simon Proud, Jay Pulli, Lise Retailleau, Annukka E. Rintamäki, Claudio Satriano, Martha K. Savage, Shahar Shani-Kadmiel, Reinoud Sleeman, Efthimios Sokos, Klaus Stammler, Alexander E. Stott, Shiba Subedi, Mathilde B. Sørensen, Taka'aki Taira, Mar Tapia, Fatih Turhan, Ben van der Pluijm, Mark Vanstone, Jerome Vergne, Tommi A.T. Vuorinen, Tristram Warren, Joachim Wassermann, Han Xiao

correspondence to: thomas.lecocq@seismology.be

This PDF file includes:

Materials and Methods
Supplementary Text (including Network Citations)
Figs. S1 to S9
References (38-55)
Caption for Movie S1
Captions for Tables S1 to S3

Other Supplementary Materials for this manuscript includes the following:

Tables S1 to S3
Movies S1

Materials and Methods

Seismic ambient noise data

In this study, we consider data from vertical seismometer components. Most traditional stations comprise broadband seismometers, whilst a handful of stations comprise short-period geophones and strong-motion accelerometers (see Supplementary Files). Analysis of a subset of stations showed that using the horizontal component data of seismometers produces similar results to those from vertical components. Since most Raspberry Shake (RS) individual and school seismometer stations (13) comprise only single, vertical-component seismic sensors, using vertical component data in our analysis allows us to combine and compare the broadband and RS datasets. To test the applicability of citizen and school seismometer stations to study lockdown effects, we demonstrate that co-located broadband and RS sensors show similar hiFSAN drops (e.g. Figs. S8, S9). The continuous seismic data processed are available from FDSN (International Federation of Digital Seismograph Network) webservices for most stations. An overview of stations and corresponding data sources are provided in the Supplementary Text and Tables.

For many countries, especially those in China and Western Europe (e.g. UK, Belgium, Germany, Switzerland), whilst the majority of stations in the corresponding national seismic networks showed noise reductions associated with lockdown, we decided not to include every station in our global analysis to try to ensure a more uniform spatial sampling. In total, we studied data from 337 seismic stations; 185 showed clear lockdown noise-reduction indications. Stations with less obvious daytime lockdown effects, but where lockdown effects are still visible at night, are also marked as lockdown stations in the Supplementary Files. For 83 stations, we did not observe any noise level decrease associated with a lockdown or in-country emergency measures. These are labelled as blue symbols in Figure 1 in the main text and are listed separately in the Supplementary Files. For 69 stations, observation of a noise level decrease was not observed due to data gaps, station hardware problems, or by masking due to longer-term seasonal effects.

Audible sound data

In Brussels, audible sound recordings are made available by the regional environment authority “Bruxelles Environnement” (<https://environnement.brussels/>; last accessed July 2020). In a preprocessing step, the audible noise is convolved with the response of the human ear in the 20 Hz - 20 kHz band.

Mobility data

Mobility data are based on proprietary mobile phone usage data from Google (38) (<https://www.google.com/covid19/mobility>, last accessed July 2020) and from Apple (<https://www.apple.com/covid19/mobility>, last accessed July 2020). These two datasets comprise anonymized daily percentage changes for a variety of different categories, such as those based on the respective mapping apps. Google data are available from 2020-02-15; Apple data from 2020-01-13. These data are likely heavily biased by members of the population carrying their phones and actively using the mapping apps. To plot the

mobility results in figures, we combine similar mobility categories from Google and Apple:

- Transport: mean of Google’s “transit stations” and Apple’s “driving” and “transit”
- Retail & recreation: mean of Google’s “grocery and pharmacy”, “retail and recreation” and “parks”
- Workplaces: Google’s “workplaces”
- Residential: Google’s “residential”

The correlation coefficient r is calculated using linear least-squares regression between each mobility time series and the seismic noise data, both expressed as “percentage changes” from baseline. The baseline is defined during the pre-lockdown period for both series.

Flight data

Flight data for Barbados were retrieved for the period Nov 2019 to May 2020 from the OpenSky net-work archive (39) over a 2.8 degree longitude by 1.6 degree latitude box centered on Grantley Adams International Airport (TBPB). This flight data is freely available to researchers upon registering at the OpenSky website. The number of take-offs and landings at TBPB was computed using the methods described in (40). For flights that operated across midnight (UTC), the flight counted for the statistics on the day of departure for take-offs or the day of arrival for landings. Due to the method of data acquisition, some flights are not included in the dataset but this does not affect the overall pattern of flight reductions due to COVID-19. A high level openly available dataset of flights from January 2020 onwards over Europe, North America and, with limitations, other parts of the world is available from OpenSky (<http://doi.org/10.5281/zenodo.3928550>) to extend our observations and interpretations for the global data set.

Noise computation approach

The quality of seismic stations is often determined using power spectral density (PSD) estimates of their records. When aggregated over hours or days, the PSD is a reasonable quantification of the noise levels in different frequency bands. Evaluations of station noise levels at different frequencies have been carried out for decades, but this has recently been made easier for continuous time series by the release of PQLX (“IRIS-PASSCAL Quick Look eXtended”) (41, 42).

For this study, we chose not to apply the default PQLX parameters (43) and apply less smoothing to obtain a finer frequency resolution together with more dynamic spectra. The PSD are computed using the ObsPy implementation (44–46), equivalent to that in PQLX. A single PSD is computed from 30-minute windows with 50 percent overlap. The PSD of each windowed time series (47) is computed using Welch’s method (48). This method reduces numerical noise in the power spectra at the expense of reducing the frequency resolution because of frequency binning, but this effect is minimized with a robust smoothing parametrization. The windowed segments are then converted to a periodogram using the squared magnitude of the discrete Fourier Transform. The displacement spectral power (D_{pow}) is related to the acceleration PSD in decibel (A_{dB}) by the following relation:

$$D_{pow}(f) = \frac{A_{pow}(f)}{(2\pi f)^2} = \frac{10^{\left(\frac{A_{dB}(f)}{10}\right)}}{(2\pi f)^2}$$

The RMS (Root-Mean-Square) of the time-domain displacement (d_{rms}), band-passed between f_{min} and f_{max} , is related to the power spectral amplitude (D_{pow}) by Parseval's identity:

$$d_{rms}(t) = \sqrt{\int_{f_{min}}^{f_{max}} D_{pow}(f) df}$$

For many stations, we tested a range of frequency bandpass filters (0.1-1.0 Hz, 1.0-20 Hz, 4-14 Hz, 4-20 Hz). Whilst the frequency spectrum of the lockdown effect might vary between different stations, we found that we were able to see the lockdown effect for most stations using the 4-14 Hz filter. The high-pass corner of the filter is set to $\gg 1$ Hz to prevent leakage of microseism, especially at island stations, many of which are included in our dataset (Figure 1). Thus, $d_{rms}(t)$ filtered between 4 and 14 Hz is the hiFSAN parameter discussed throughout the text. This frequency range allowed us to obtain a large dataset of noise changes, especially enabling 40 samples per second at higher data to be analyzed. Where only 20 samples per second seismic data were available for a handful of stations, data were bandpass filtered between 4 and 9 Hz. HE.HEL2 in Helsinki, Finland, is the only station for which $d_{rms}(t)$ reduction was only visible between 60 and 90 Hz.

A standardized processing strategy and parametrization was defined in order to obtain global comparable results. Our processing workflow is as follows:

- selecting the seismic channel and data provider of the seismometer data of interest;
- downloading the seismic waveform data for the time period of interest;
- computing daily probabilistic PSDs (PPSD) from the downloaded data;
- processing PPSDs and extracting the RMS of the time-domain displacement of the selected time period for different frequency bands;
- manual assessment of long-term hiFSAN;
- creating data analysis figures to demonstrate noise variation over time using different visualizations (pre-lockdown and lockdown hourly displacement variation, monthly variation). Figures were made using Matplotlib (49).

Due to the heterogeneity of global seismic networks and the vast quantity of data downloading and processing required, we invited members of the seismological community via social media and traditional word-of-mouth in a democratized scientific approach (50). All authors have accessed and processed seismic data following the data analysis instructions presented in the Methods Section. All authors have read and commented during the development of this manuscript. This processing workflow has been made publicly available in Jupyter Notebooks (51) published on GitHub (52); (<https://github.com/ThomasLecocq/SeismoRMS>; last accessed July 2020). The final notebooks will be added to seismo-live.org (53).

In this paper, we focus on computing changes in ground displacement. Similar results have been obtained by computing velocity or acceleration noise changes. For

plotting the global comparisons in Figure 2 and Figure S1, data are normalized to the 15-85th percentiles of the pre-lockdown period and clipped above the 99th percentile for remaining outliers.

References

38. A. Aktay, et al., arXiv preprint arXiv:2004.04145(2020).
39. M. Schäfer, M. Strohmeier, V. Lenders, I. Martinovic, M. Wilhelm, IPSN-14 Proceedings of the 13th International Symposium on Information Processing in Sensor Networks (IEEE, 2014), pp. 83–94.
40. S. R. Proud, Aerospace 7, 16 (2020).
41. D. E. McNamara, R. P. Buland, Bulletin of the Seismological Society of America 94, 1517 (2004).
42. D. E. McNamara, R. I. Boaz, U.S. Geol. Surv. Open-File Rept 2010-1292, 41 (2010).
43. R. E. Anthony, A. T. Ringler, D. C. Wilson, M. Bahavar, K. D. Koper, Seismological Research Letters (2020).
44. M. Beyreuther, et al., Seismological Research Letters 81, 530 (2010).
45. T. Megies, M. Beyreuther, R. Barsch, L. Krischer, J. Wassermann, Annals of Geophysics 54, 47 (2011).
46. L. Krischer, et al., Computational Science & Discovery 8, 014003 (2015).
47. R. B. Blackman, J. W. Tukey, Bell System Technical Journal 37, 185 (1958).
48. P. Welch, IEEE Transactions on Audio and Electroacoustics 15, 70 (1967).
49. J. D. Hunter, Computing in Science & Engineering 9, 90 (2007).
50. R. Lacassin, et al., Geoscience Communication 3, 129 (2020).
51. T. Kluyver, et al., Positioning and Power in Academic Publishing: Players, Agents and Agendas, F. Loizides, B. Schmidt, eds. (IOS Press, 2016), pp. 87–90.
52. T. Lecocq, F. Massin, C. Satriano, M. Vanstone, T. Megies, SeismoRMS - A simple python/jupyter notebook package for studying seismic noise changes (2020).
53. L. Krischer, et al., Seismological Research Letters 89, 2413 (2018).
54. Center for International Earth Science Information Network - CIESIN - Columbia University, Gridded population of the world, version 4 (gpwv4): Population density, revision 11 (2018).
55. QGIS Development Team, QGIS Geographic Information System, Open Source Geospatial Foundation (2020).

Supplementary Text

Citations for seismic networks used in this study

This section lists the network codes (in bold) for stations analyzed in this study followed by the full citation as per the FDSN website, where available.

- **AC**: Institute of Geosciences, Energy, Water and Environment. (2002). Albanian Seismological Network [Data set]. International Federation of Digital Seismograph Networks. <https://doi.org/10.7914/SN/AC>

- **AF:** Penn State University. (2004). AfricaArray. International Federation of Digital Seismograph Networks. <https://doi.org/10.7914/SN/AF>
- **AK:** Alaska Earthquake Center, U. O. A. F. (1987). Alaska Regional Network. International Federation of Digital Seismograph Networks. <https://doi.org/10.7914/SN/AK>
- **AM:** (1) Raspberry Shake Community; (2) OSOP, S.A.; (3) Gempa GmbH. (2016). Raspberry Shake. (1) OSOP, S.A.; (2) gempa GmbH. <https://doi.org/10.7914/SN/AM>
- **AM,** Nepal: Nepal School Seismology Network, (1) <http://dx.doi.org/10.5281/zenodo.3406345> and (2) Subedi S, Hetényi G, Denton P, Sauron A (2020) Seismology at School in Nepal: A program for educational and citizen seismology through a low-cost seismic network. *Front Earth Sci* 8:73. doi:10.3389/feart.2020.00073.
- **AU:** Geoscience Australia (GA). (1994). Australian National Seismograph Network (ANSN).
- **BE:** Royal Observatory of Belgium (1985). Belgian Seismic Network. International Federation of Digital Seismograph Networks. <https://doi.org/10.7914/SN/BE>
- **BK:** Northern California Earthquake Data Center. (2014). Berkeley Digital Seismic Network (BDSN) [Data set]. Northern California Earthquake Data Center. <https://doi.org/10.7932/BDSN>
- **BL:** Universidade de Sao Paulo, USP. (1988). Brazilian Lithospheric Seismic Project (BLSP).
- **BW:** Department of Earth and Environmental Sciences, Geophysical Observatory, Ludwig-Maximilians-Universität München (2001), BayernNetz. International Federation of Digital Seismograph Networks. <https://doi.org/10.7914/SN/BW>.
- **BX:** Department of Geological Survey of Botswana. (2001). Botswana Seismological Network (BSN).
- **CI:** Universidad de Chile. (2013). Red Sismologica Nacional. International Federation of Digital Seismograph Networks. <https://doi.org/10.7914/SN/CI>
- **CA:** Institut Cartogràfic I Geològic De Catalunya, Institut d'Estudis Catalans (1984). Catalan Seismic Network [Data set]. International Federation of Digital Seismograph Networks. <https://doi.org/10.7914/SN/CA>
- **CH:** Swiss Seismological Service (SED) At ETH Zurich. (1983). National Seismic Networks of Switzerland. ETH Zürich. <https://doi.org/10.12686/sed/networks/ch>
- **CI:** California Institute of Technology and U.S. Geological Survey (USGS) Pasadena. (1926). Southern California Seismic Network. International Federation of Digital Seismograph Networks. <https://doi.org/10.7914/SN/CI>
- **CN:** Geological Survey of Canada. (1989). Canadian National Seismograph Network. International Federation of Digital Seismograph Networks. <https://doi.org/10.7914/SN/CN>
- **CQ:** Geological Survey Department Cyprus. (2013). Cyprus Broadband Seismological Network. International Federation of Digital Seismograph Networks. <https://doi.org/10.7914/SN/CQ>

- **CU:** Albuquerque Seismological Laboratory (ASL)/USGS. (2006). Caribbean USGS Network. International Federation of Digital Seismograph Networks. <https://doi.org/10.7914/SN/CU>
- **EI:** INSN. (1993). Irish National Seismic Network, operated by the Dublin Institute for Advanced Studies and supported by the Geological Survey Ireland. International Federation of Digital Seismograph Networks. <https://doi.org/10.7914/SN/EI>
- **FR:** RESIF. (1995). RESIF-RLBP French Broad-band network, RESIF-RAP strong motion network and other seismic stations in metropolitan France [Data set]. RESIF - Réseau Sismologique et géodésique Français. <https://doi.org/10.15778/RESIF.FR>
- **G:** Institut de Physique du Globe de Paris (IPGP), & Ecole et Observatoire des Sciences de La Terre de Strasbourg (EOST). (1982). GEOSCOPE, French Global Network of broadband seismic stations. Institut de Physique du Globe de Paris (IPGP). <https://doi.org/10.18715/GEOSCOPE.G>
- **GB:** British Geological Survey. (1970). Great Britain Seismograph Network. Contains British Geological Survey materials © UKRI [2020].
- **GE:** GEOFON Data Centre. (1993). GEOFON Seismic Network. Deutsches GeoForschungsZentrum GFZ. <https://doi.org/10.14470/TR560404>
- **GO:** Iliia State University- Seismic Monitoring Centre of Georgia (Georgia). (1988). National Seismic Network of Georgia.
- **GR:** Federal Institute for Geosciences and Natural Resources (BGR). (1976). German Regional Seismic Network (GRSN). Federal Institute for Geosciences and Natural Resources (BGR). <https://doi.org/10.25928/mbx6-hr74>
- **GT:** Albuquerque Seismological Laboratory (ASL)/USGS. (1993). Global Telemetered Seismograph Network (USAF/USGS). International Federation of Digital Seismograph Networks. <https://doi.org/10.7914/SN/GT>
- **HE:** Institute of Seismology, U. O. H. (1980). The Finnish National Seismic Network. GFZ Data Services. <https://doi.org/10.14470/UR044600>
- **HL:** National Observatory of Athens, I. O. G. (1997). National Observatory of Athens Seismic Network. International Federation of Digital Seismograph Networks. <https://doi.org/10.7914/SN/HL>
- **HT:** Aristotle University of Thessaloniki Seismological Network. (1981). Permanent Regional Seismological Network operated by the Aristotle University of Thessaloniki. International Federation of Digital Seismograph Networks. <https://doi.org/10.7914/SN/HT>
- **IC:** Albuquerque Seismological Laboratory (ASL)/USGS. (1992). New China Digital Seismograph Network. International Federation of Digital Seismograph Networks. <https://doi.org/10.7914/SN/IC>
- **II:** Scripps Institution of Oceanography. (1986). IRIS/IDA Seismic Network. International Federation of Digital Seismograph Networks. <https://doi.org/10.7914/SN/II>
- **IM:** (1965). International Miscellaneous Stations (IMS).
- **IN:** India Meteorological Department. (2000). National Seismic Network of India.

- **IU:** Albuquerque Seismological Laboratory (ASL)/USGS. (1988). Global Seismograph Network (GSN - IRIS/USGS). International Federation of Digital Seismograph Networks. <https://doi.org/10.7914/SN/IU>
- **IV:** INGV Seismological Data Centre. (2006). Rete Sismica Nazionale (RSN). Istituto Nazionale di Geofisica e Vulcanologia (INGV), Italy. <https://doi.org/10.13127/SD/X0FXnH7QfY>
- **KO:** Bogazici University Kandilli Observatory and Earthquake Research Institute. (2001). Bogazici University Kandilli Observatory and Earthquake Research Institute. International Federation of Digital Seismograph Networks. <https://doi.org/10.7914/SN/KO>
- **KV:** Oth, A., Barrière, J., D'Oreye, N., Mavonga, G., Subira, J., Mashagi, N., Kafundu, B., Fiama, S., Celli, G., De Dieu Birigande, J., Ntenge, A. J., & Kervyn, F. (2013). Kivu Seismological Network (KivuSnet). Deutsches GeoForschungsZentrum GFZ. <https://doi.org/10.14470/XI058335>
- **LD:** Lamont Doherty Earth Observatory (LDEO), Columbia University. (1970). Lamont-Doherty Cooperative Seismographic Network (LCSN). <https://doi.org/10.7914/SN/LD>
- **MD:** Geological and Seismological Institute of Moldova. (2007). Moldova Digital Seismic Network. International Federation of Digital Seismograph Networks. <https://doi.org/10.7914/SN/MD>
- **MN:** MedNet Project Partner Institutions. (1990). Mediterranean Very Broadband Seismographic Network (MedNet). Istituto Nazionale di Geofisica e Vulcanologia (INGV). <https://doi.org/10.13127/SD/fBBBtDtd6q>
- **MQ:** Institut de Physique du Globe de Paris. (1935) The data used in this study were acquired by the Volcanological and Seismological of Martinique (OVSM) via the VOLOBISIS Portal : <http://volobsis.ipgp.fr>.
- **MX:** SSN (2017). Servicio Sismológico Nacional, Instituto de Geofísica, Universidad Nacional Autónoma de México, México. <https://doi.org/10.21766/SSNMX/SN/MX>
- **NC:** USGS Menlo Park. (1967). USGS Northern California Network. International Federation of Digital Seismograph Networks. <https://doi.org/10.7914/SN/NC>
- **NE:** Albuquerque Seismological Laboratory (ASL)/USGS. (1994). New England Seismic Network. International Federation of Digital Seismograph Networks. <https://doi.org/10.7914/SN/NE>
- **NL:** KNMI. (1993). Netherlands Seismic and Acoustic Network. Royal Netherlands Meteorological Institute (KNMI). <https://doi.org/10.21944/e970fd34-23b9-3411-b366-e4f72877d2c5>
- **NP:** USGS Earthquake Science Center. (1931). U.S. National Strong-Motion Network. International Federation of Digital Seismograph Networks. <https://doi.org/10.7914/SN/NP>
- **NS:** University of Bergen (1982), Norwegian National Seismic Network.
- **NZ:** Institute of Geological & Nuclear Sciences Ltd (GNS New Zealand). (1988). New Zealand National Seismograph Network. We acknowledge the New Zealand GeoNet project and its sponsors EQC, GNS Science and LINZ, for providing data/images used in this study.

- **OE:** ZAMG-Zentralanstalt Für Meteorologie Und Geodynamik. (1987). Austrian Seismic Network. International Federation of Digital Seismograph Networks. <https://doi.org/10.7914/SN/OE>
- **PA:** Red Sismica Volcan Baru. (2000). ChiriNet [Data set]. International Federation of Digital Seismograph Networks. <https://doi.org/10.7914/SN/PA>
- **PF:** Institut de Physique du Globe de Paris (1980). Piton de la Fournaise Volcano Observatory Network (Reunion Island) (OVPF). The data used in this study were acquired by the Volcanological and Seismological of Observatory of Piton de la Fournaise (OVPF) via the VOLOBSIS Portal : <http://volobsis.ipgp.fr>.
- **PT:** Pacific Tsunami Warning Center (1965). Pacific Tsunami Warning Seismic System
- **QM:** Bureau de Recherches Géologiques et Minières (BRGM). (2019). Comoros Seismic Network (Comoros Seismic Network). The Mayotte station KNKL (QM) was installed through Tellus Mayotte project (CNRS-INSU) and its data was made available to LR through REVOSIMA.
- **OV:** Protti, M. (1984). Observatorio Vulcanológico y Sismológico de Costa Rica [Data set]. International Federation of Digital Seismograph Networks. <https://doi.org/10.7914/SN/OV>.
- **RO:** National Institute for Earth Physics (NIEP Romania). (1994). Romanian Seismic Network. International Federation of Digital Seismograph Networks. <https://doi.org/10.7914/SN/RO>
- **S1:** Australian National University (ANU, Australia). (2011). Australian Seismometers in Schools [Data set]. Australian Passive Seismic Server - Australian National University. <https://doi.org/10.7914/SN/S1>.
- **SV:** Servicio Nacional de Estudios Territoriales (SNET El Salvador). (2004). Servicio Nacional de Estudios Territoriales (SNET), El Salvador (SNET-BB)
- **TC:** (2016). Universidad de Costa Rica. <https://doi.org/10.15517/TC>
- **US:** Albuquerque Seismological Laboratory (ASL)/USGS. (1990). U.S. National Seismic Network. International Federation of Digital Seismograph Networks. <https://doi.org/10.7914/SN/US>
- **YS:** Diaz, J., and Schimmel, M. (2019). SANIMS [Data set]. International Federation of Digital Seismograph Networks. https://doi.org/10.7914/SN/YS_2019

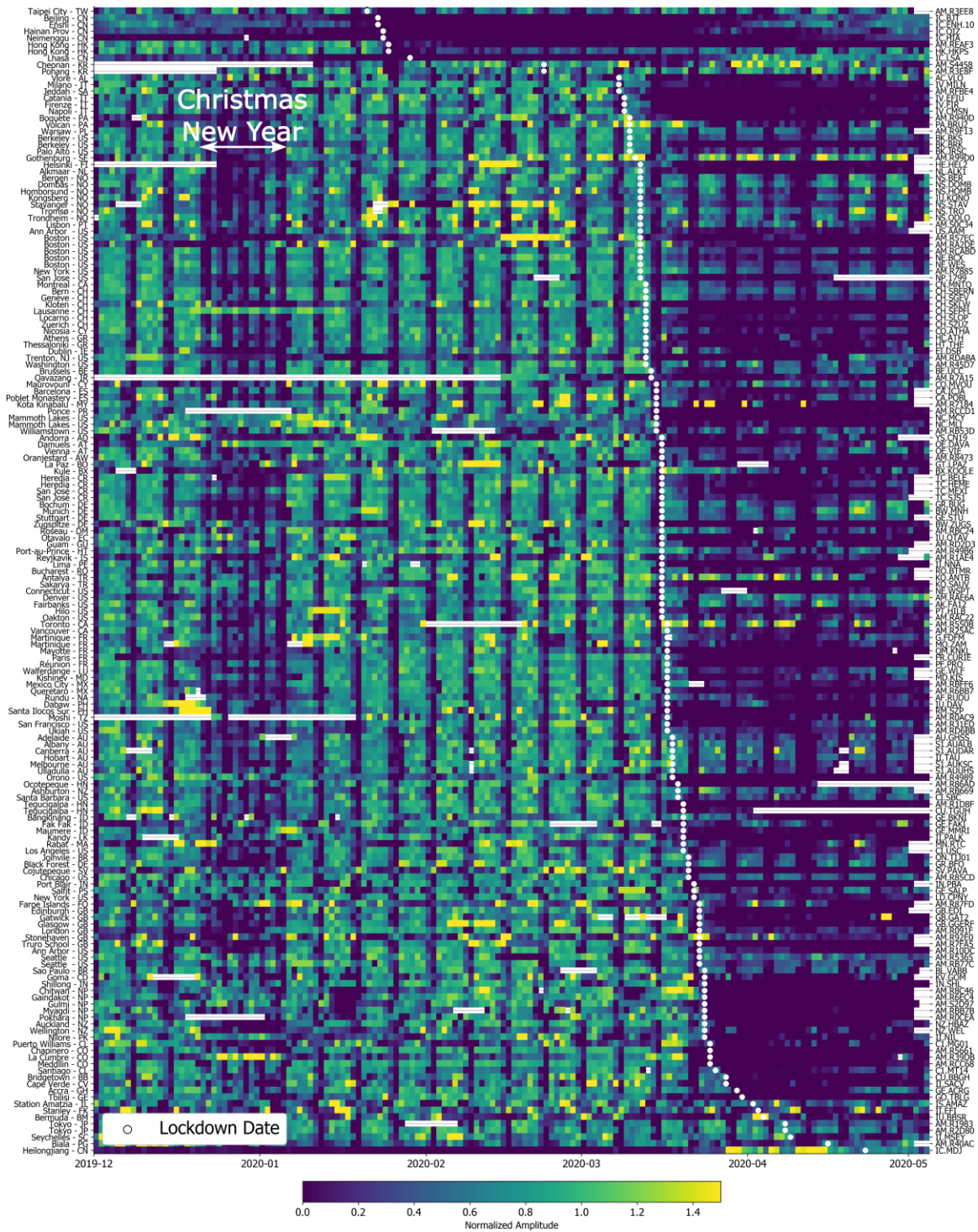


Fig. S1. Global temporal changes in seismic noise.

Global daily median hiFSAN based on displacement data, normalized to percentage variation of the baseline before lockdown measures, and sorted by lockdown date. Data gaps are colored white. Location and country code of the station are indicated on the left; network and station codes on the right. Stations with long data gaps over the period are not shown.

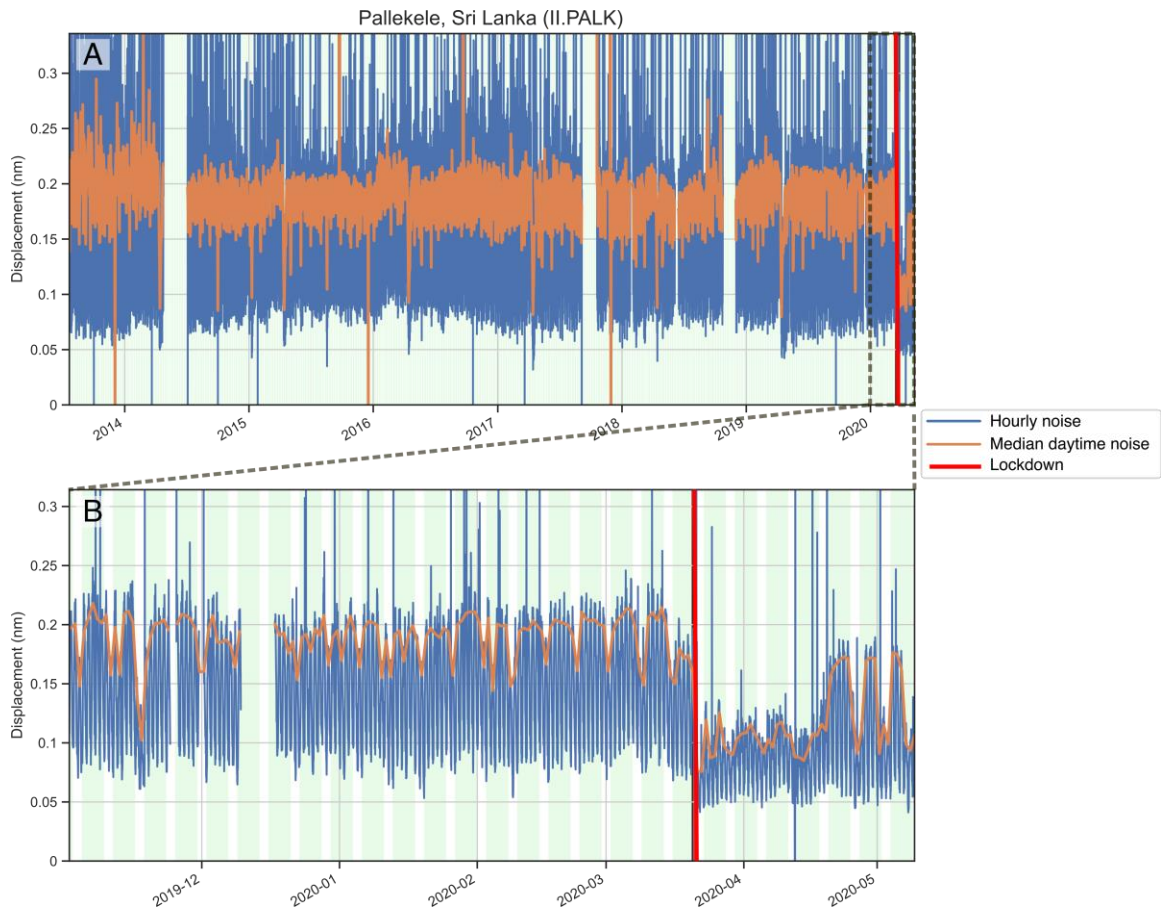


Fig. S2. Long term evolution of hiFSAN in Sri Lanka.
 A) Long term seismic noise evolution. B) Zoom-in of noise in 2020.

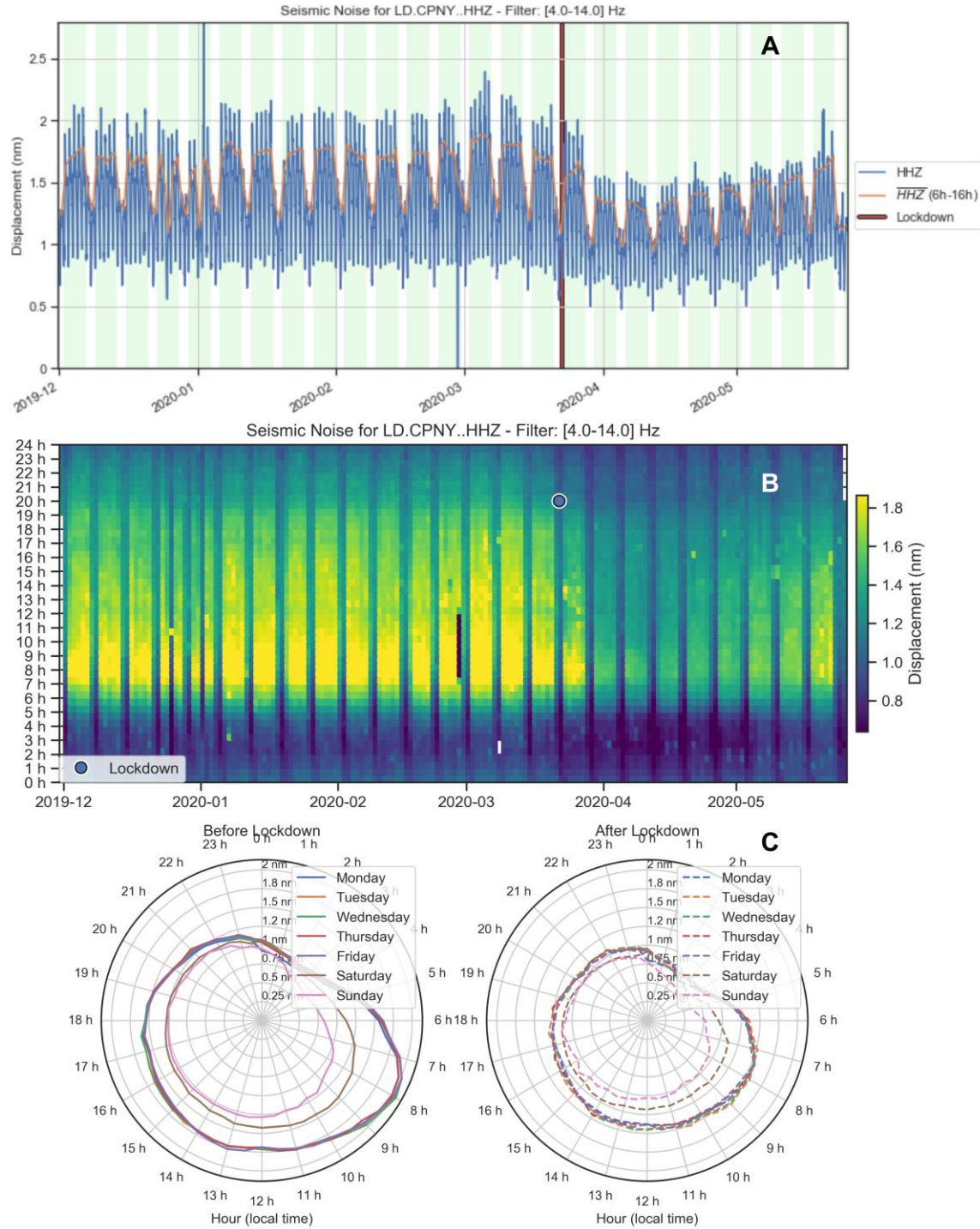


Fig. S3. Lockdown effects on seismic noise in Central Park, NY.

(A) Evolution of seismic noise at station LD.CPNY in Central Park, New York for the Dec 2019 - May 2020 period based on displacement data. (B) The same as (A) but shown in an hourly grid representation. (C) 24h clock plots showing average displacement variation for each day of the week for the period before lockdown (left) and after lockdown started (right).

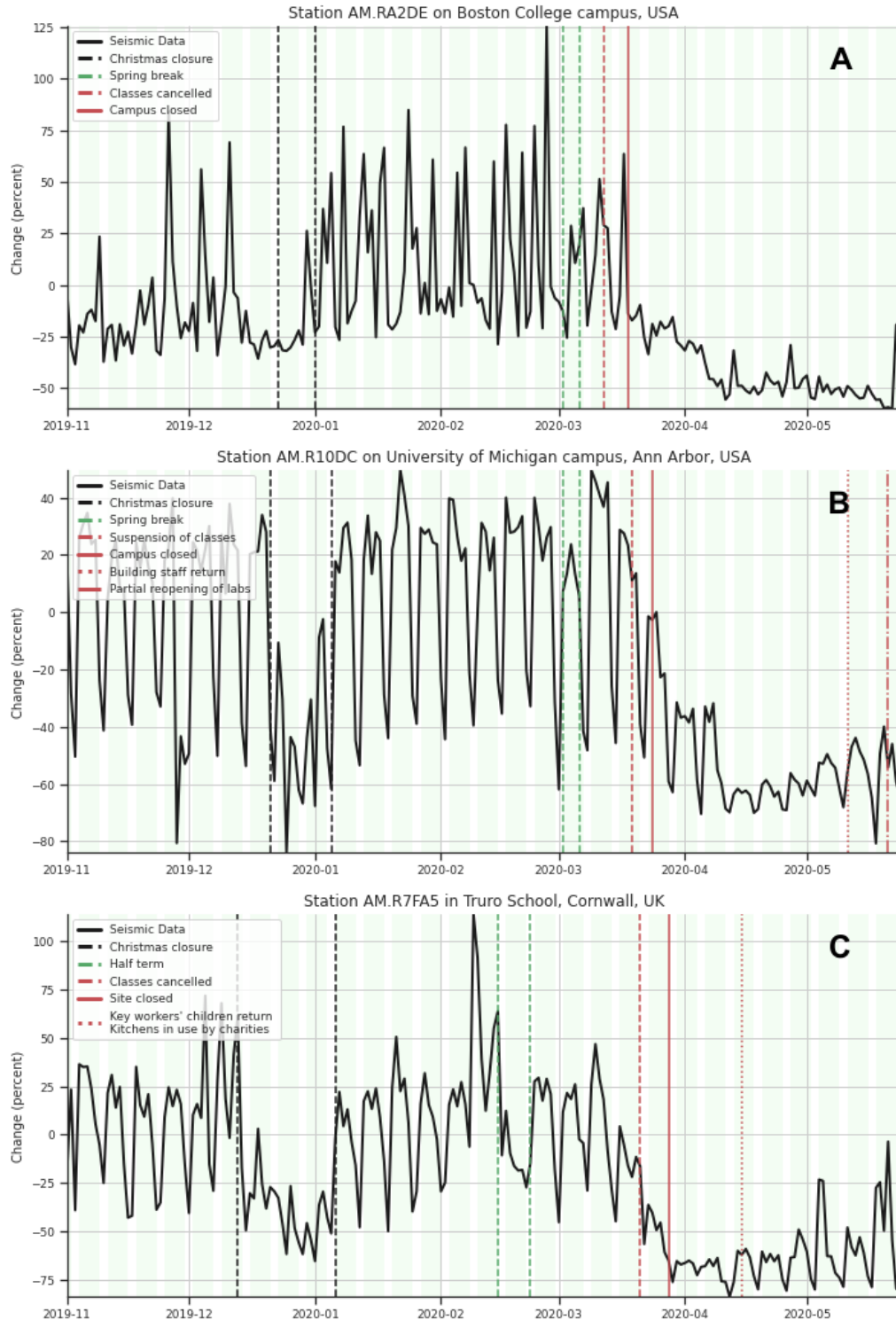


Fig. S4. Temporal changes in hiFSAN at schools and universities.

(A) Boston College (US). (B) University of Michigan campus (US). (C) Truro School (Cornwall, UK). Time periods like the Christmas break and Spring break / half term are easily identified as periods of lower seismic noise. Note the large drop in hiFSAN up to more than 50 % change after classes are cancelled and campuses are closed.

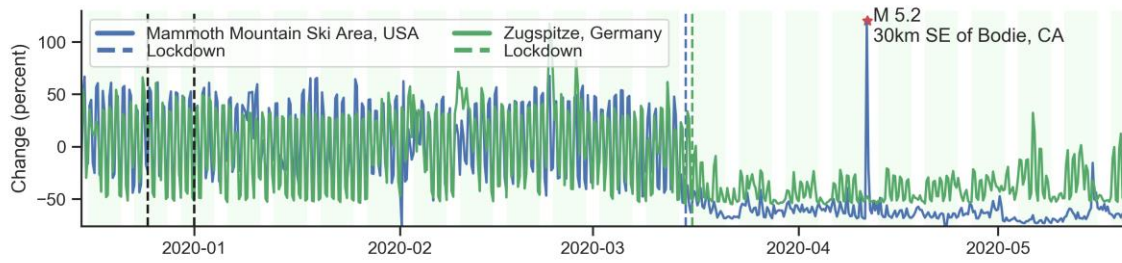


Fig. S5. Lockdown effects on seismic noise in touristic ski resort areas.

Temporal changes of hiFSAN at two touristic ski resort areas: Mammoth Mountain (USA - station NC.MCY) and Zugspitze (Germany, station BW.ZUGS), showing the effect of the complete stop of the resorts' lifts or cog-wheel railway

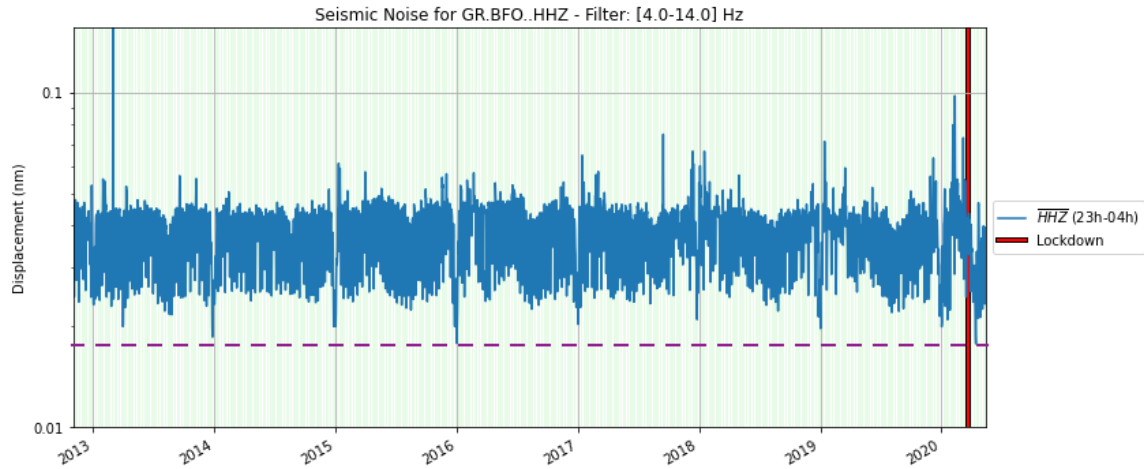


Fig. S6. Temporal changes in hiFSAN at the Black Forest Observatory, Germany.

Long-term noise evolution at the Black Forest Observatory, Germany (GR.BFO) based on median nighttime (23:00-04:00) RMS noise from displacement data. The purple dashed line indicates the minimum noise observed during the 2020 lockdown period. Note the logarithmic y-axis.

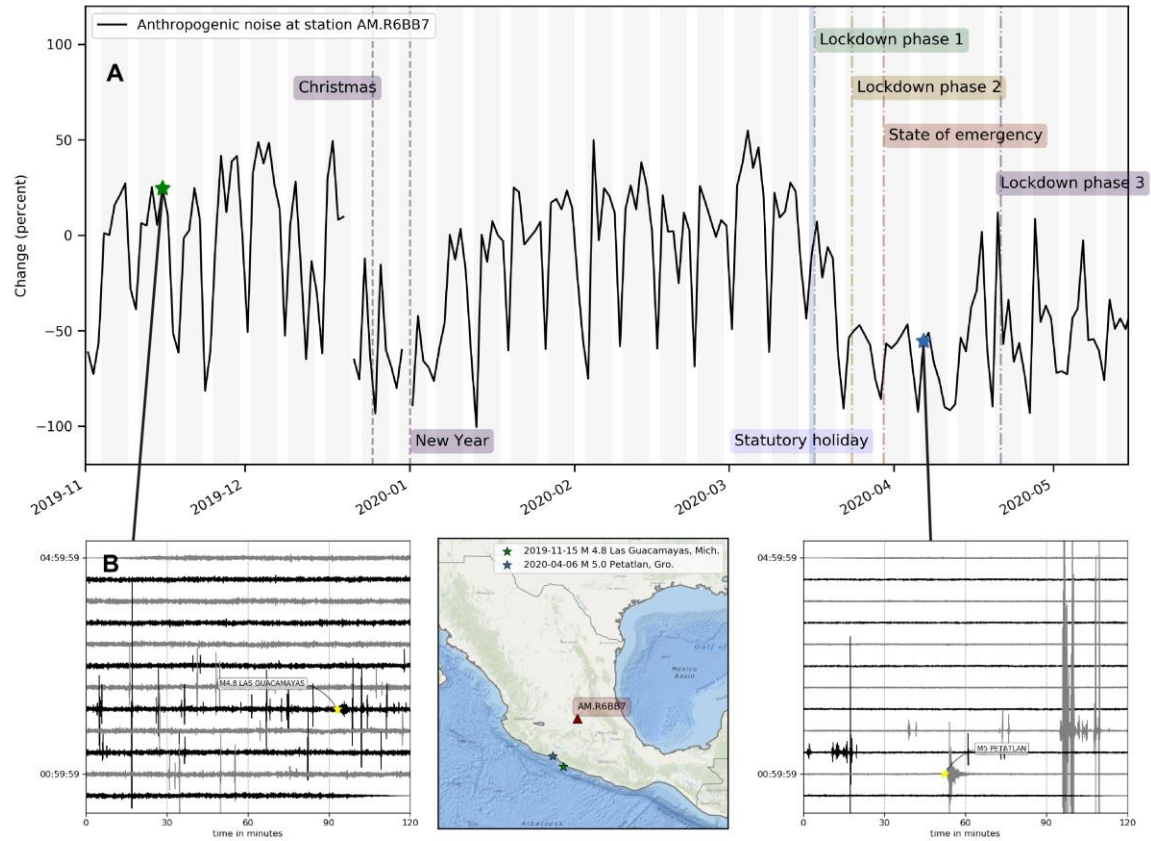


Fig. S7. Increased earthquake detection capability in Mexico.

(A) Temporal changes in hiFSAN at Raspberry Shake station AM.R6BB7 (city center of Querétaro, Mexico). (B) Earthquakes at Las Guacamayas (15/11/2019, M4.8 and 28 km depth) and Petatlan (07/04/2020, M5.0 and 15 km depth) recorded before (left column) and after the lockdown (right). The insert in the center indicates the locations of the earthquakes and Raspberry Shake station.

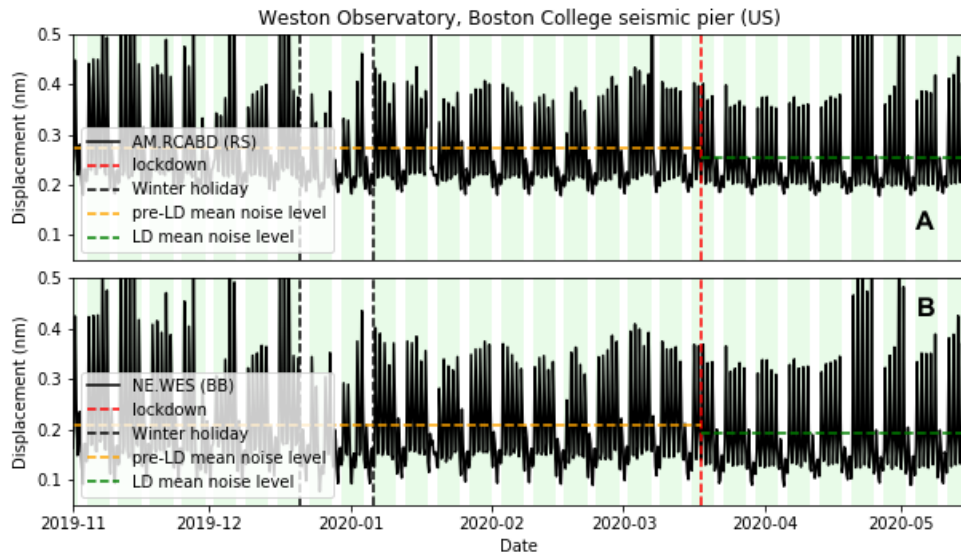


Fig. S8. Comparison of lockdown effects on Raspberry Shake and broadband stations on the surface.

Temporal changes in seismic noise at the co-located AM.RCABD Raspberry Shake station (A) and NE.WES broadband station (B) at the Weston Observatory, Boston College seismic pier in the United States of America.

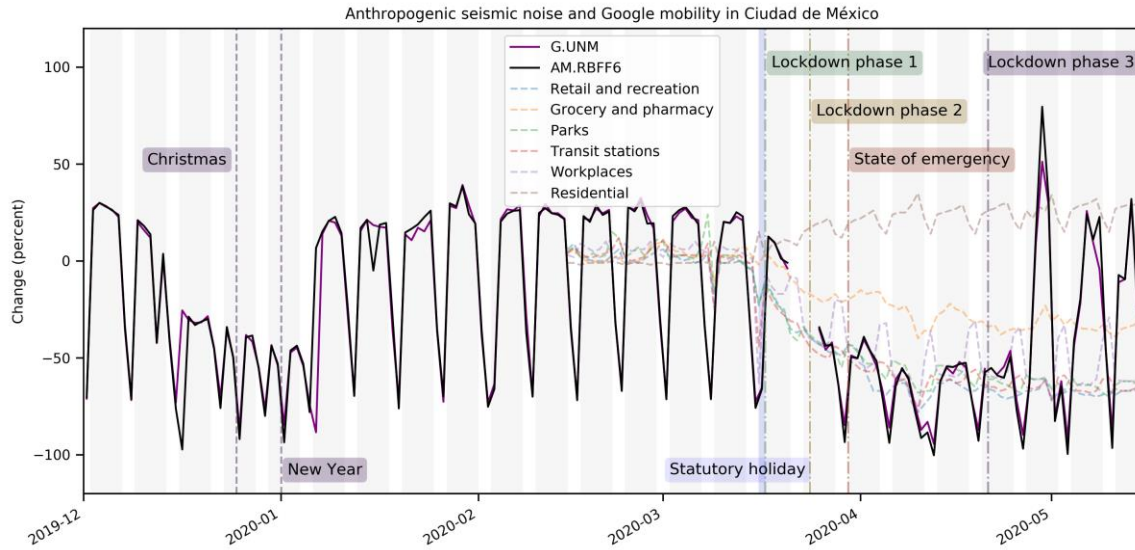


Fig. S9. Comparison of lockdown effects on Raspberry Shake and broadband stations in a borehole.

Temporal changes in hiFSAN at broadband station G.UNM and Raspberry Shake station AM.RBFF6, both installed in a 20m deep borehole in the Ciudad Universitaria in Mexico City. The evolution of Google mobility data for the city are shown for comparison as dashed lines.

Movie S1

Movie version of Figure 2 and Figure S1. The time evolution of the amplitude of hiFSAN for each station is shown as bars with variable height. The lockdown dates (LD1) for each country appear on the left side.

Introduction to the Tables

The supplementary tables give an overview of the seismic stations for which data were analyzed in this study. Each author provided lockdown (LD) information (DateLD1, TimeLD1, DateLD2, TimeLD2) for the seismometer location. Population density data show interpolated estimates of human population count for the year 2020 (54). These grid data are consistent with national census and population registers. *popden30s* gives population counts within 30 arc-second grid cells (cell size of roughly 1 km at the equator); *popden2.5min* gives population counts within 2.5 arc-minute grid cells (cell size of roughly 5 km at the equator; the inverse of this data column is used in Fig. 1). Population data for each station were extracted from grid data using QGIS (55). Station locations (latitude, longitude) in all tables were extracted from FDSN websites. The three files contain:

Additional Data table S1 (separate file)

Stations where lockdown noise reduction was observed; these 185 stations are shown in Figures 1 and 4 and in Figure S1; 'yes' in *columnplottedinfig2* indicates that the station was displayed in Figure 2; 'No/double' means that another close by station in the area of interest is used;

Additional Data table S2 (separate file)

Stations where lockdown noise reduction was not observed. These 83 stations are also shown in Figure 1;

Additional Data table S3 (separate file)

Stations where data gaps, station hardware problems, or longer-term seasonal effects prohibited a conclusion on noise changes. These 69 stations are not plotted in Figure 1.